Transparent PEM-FC Performance Analysis under the Optimal Clamping Pressure Applied at its Bolts

B. Srinivasarao
Assistant Professor, Department of EEE, Aditya Institute of Technology and Management, Tekkali, Andhra Pradesh, India, Email: bsreee2013@gmail.com.

Mohammad Aasim Khan
Assistant Professor, Department of Mathematics & Statistics, Integral University, Lucknow, India, Email: khan.aasim012@gmail.com.

E V Naga Lakshmi
Associate Professor ECE Department MVSR Engineering College, Hyderabad, Telangana, India, Email: nagalakshmi_ece@mvsrec.edu.in.

P. Venkata Prasad
Professor, Department of EEE, Chaitanya Bharathi Institute of Technology, Hyderabad, Telangana, India, Email: pvprasad _eee@cbit.ac.in.

Smruti Ranjan Nayak
Assistant Prof., Department of EEE, Centurion University, Bhubaneswar, Odisha, India, Email: smrutiranjan@cutm.ac.in.

Krishna Chaithanya Janapati
Associate Professor, Vardhaman College of Engineering, Department of ECE, Hyderabad, Telangana, India, Email: janapatikrishnachaithanya@gmail.com.

Edrees Yahya Alhawsawi
Senior Researcher, Oakland University, Department: Electrical and Computer Engineering, Michigan, USA, Email: ealhawsawi@oakland.edu.

Thresia Michael
University Centre of Research and Development, Chandigarh University, Gharuan, Mohali, Punjab, India, Email: thresiamichael2203@gmail.com.

Ajay Sudhir Bale*
Senior Assistant Professor, Department of ECE, New Horizon College of Engineering, Bangalore, Karnataka, India, Email: ajaysudhirbale2@gmail.com.

Abstract: Fuel cells are gaining their attention recently due to the increasing of their applications in various sectors. The study involved conducting experiments on a titanium gas distributor plates (GDPs) equipped single transparent proton exchange membrane fuel cell (PEM-FC). This research focuses on analyzing how various factors influence the performance of PEM-FC, including clamping pressure, which is determined by the applied torque to each bolt, the humidification temperatures of both the cathode and anode, the overall temperature of the PEM-FC, and the flow rate of the cathode. The findings indicate that the performance of the PEM-FC initially increases to a maximum point before declining with further increases in torque at bolts. Additionally, it was observed that as the humidification temperature of the cathode rises, the performance of the PEM-FC decreases, whereas an increase in the temperature of the PEM-FC itself can be able to improve performance. Furthermore, the reactant for humidification of the anode is crucial for enhancing the efficiency of PEM-FC. While the impact of the flow rate at cathode is minimal in the ohmic overpotential and activation regions, it becomes significantly important in the concentration overpotential region.

Keywords: Fuel Cells, PEM-FC, Overpotential, Gas diffusion layer, Humidification temperature.

I. Introduction

Since last few decades, there has been a viable surge in interest regarding the performance of PEM-FCs due to increasing the application of PEM-FCs in various sectors including power, hospitals, vehicles, etc. The PEM-FCs can able to produce required electricity by utilizing Hydrogen and Oxygen. This heightened attention can be attributed to their numerous advantages, which include operating at low temperatures, delivering high power density, producing zero emissions, and featuring a compact and lightweight design [1-3]. Additionally, PEM-FCs are recognized for their exceptional capabilities in both starting up and shutting down efficiently. A typical PEM-FC is composed of several key components: end plate, gas diffusion layers (GDLs), current collectors, GDPs, gaskets, and a proton exchange membrane. These components are tightly assembled through a process of high compression, which serves a dual purpose. Firstly, it ensures that contact resistances remain low, and secondly, it effectively prevents any gas leakages, thereby enhancing overall performance. While it is generally observed that increasing compression can lead to improved electrical conductivity within the PEM-FC, this same compression can also pose challenges. Specifically, it may hinder the transport of gases and the removal of water by altering the distribution of pore sizes within the cell. The impact of compression on the performance of PEM-FCs has been the subject of investigation by numerous research teams, as documented in various studies [1-2].

The thicknesses of the gasket and the GDLs, as well as its porosity, are influenced by the torque applied to the 4 bolts. Additionally, electrical contact resistance of layers is depending on how much the layers compressed due to the applied torque on the bolts. The water management and performance within the PEM-FC can be effected by humidification, temperature, reactant gas flow rates, and the properties of the GDL. All of these factors are linked to the compressive force exerted on the membrane electrode assembly (MEA). Therefore, understanding how those components impact the operation of PEM-FC is essential for improving its performance. Among these elements, the properties of the GDL and the design of the GDPs are particularly important, as they cannot be altered during the operation of PEM-FC and must be meticulously considered during the manufacturing process.

Numerous scholars are examined the impact of clamping pressure by imposed torque to every bolt on the fabrication process on different parameters of PEM-FC. The authors referenced in [4-6] explored how variations in torque affect the performance of PEM-FCs and identified an optimal torque on bolt. Ge et al. [7] conducted an experimental research on the influence of GDL compression on the PEM-FCs performance, focusing on both types of

GDL materials: TORAY™ carbon fibre paper and ELAT carbon cloth by double micro-diffusion layers, which had an additional micro-diffusion layer on the surface in contact with the catalyst layer. Their findings indicated that the performance of the fuel cell, as illustrated by the polarization curve, initially improved and subsequently declined with increasing compression force beyond a certain threshold. Researchers in [8-9] numerically analyzed the effect of clamping force on PEM-FC performance and reported as there exists a maximum density of power corresponding to an optimal torque applied to the bolts of the PEM-FC. The experimental investigation conducted by the authors in [10] revealed that the permeability and porosity of the GDL, as well as the resistance due to electrical contact between the GDL and GDPs, decreased with an increase in clamping pressure. Additionally, the authors in [11-12] found through experimental means that performance increased and later decreased with pressure across two regions of polarization: the mass transport and ohmic regions of the PEM-FC. The advantages of achieving distribution of uniform pressure within a single PEM-FC and across a stack were stated by the authors in [13] through the use of newly designed end plates. Furthermore, the authors in [14] experimentally determined that enhancing the compression of the GDL led to a reduction in pore volume, thereby facilitating high-quality contact between the other components and carbon fibres in the GDL.

Most researchers have chosen stainless steel for GDPs due to its thin profile, strong mechanical properties, and the clear distinction it provides between the GDL and the distributor plates. This makes it particularly suitable for transparent PEM-FCs. However, the stability of stainless steel under chemicals is limited, which can hinder long-term performance [15-16]. To overcome this limitation, gold-plated stainless steel is being utilized as a solution. This research employs plates designed by titanium with a single serpentine flow pattern, which serve as GDPs. These plates are chosen for their proven high thermal and electrical conductivities, making them ideal for this application [17-20]. Moreover, titanium is known for its exceptional chemical stability typical of PEM-FC's operating temperature, especially when compared to stainless steels. This characteristic is crucial for maintaining performance and longevity in fuel cell applications. Additionally, titanium boasts a remarkable strength-to-weight ratio, which is advantageous in reducing the overall weight of the system. The use of titanium also allows for a thinner design, creating a clear distinction between the GDL and the distributor plates, which can enhance the efficiency of gas distribution within the PEM-FC.

This research work began with an emphasis on enhancing the clamping pressures evaluated by the torque exerted on every bolt of the transparent PEM-FCs. Following this initial optimization, the performance of the PEM-FC is thoroughly evaluated under the newly established clamping pressure. This evaluation involved fine-tuning various operating parameters of the PEM-FC, such as the humidification temperatures for anode and cathode, the flow rates of the cathode, and the overall temperatures within the cell [21-25].

II. Experimental Setup

The transparent PEM-FC developed in this research includes several key components: a MEA, transparent cover plates, gaskets, flow field plates, and end plates, as depicted in Figure 1(a). The MEA will be constructed with a N212 Nafion membrane sandwiched among cloths of carbon fiber, which are characterized by their mechanical strength, lightweight nature, and high permeability. The platinum catalyst used in the fuel cell exhibits a significantly lower activity for the reaction due to reduction of oxygen when compared to the reaction due to oxidation of hydrogen. This disparity highlights the necessity for a much greater amount of platinum to be loaded in the cathode than in the anode. As a result, the platinum loading for the anode is set at 0.25 mg/cm^2, while the cathode is loaded with platinum at a higher intensity of 0.50mg/cm^2. The MEA, which has a surface area of 25.0cm^2, is positioned between two GDPs manufactured by sing titanium. This material is chosen for its outstanding electrical conductivity and chemical stability, and it also serves the dual purpose of acting as a collector for current.

The channels within both cathode and anode plates of the GDP for gas flow are designed in a continuous serpentine pattern. Each channel measures 2.0mm in width and 1.0mm in depth, with ribs also measuring 2.0mm in width, as depicted in Figure 1(b). To enhance the temperature of the cell, the extension areas of the titanium plates are attached by heater coils on either side. These extension areas also serve as fins, helping to dissipate heat through natural or forced convection when the temperature exceeds a specified threshold. A copper contactor will be mounted on one side of the extension place to maintain the operated temperature of PEM-FC. To ensure the correct force due to compression, prevent the leakage through the MEA, and provide insulation between the cathode and anode of GDPs, silicone rubber papers, each 0.3mm thick, are placed on MEA's two sides. To allow for the observation of flow of water distribution behavior within the flow channels, each 5 mm thick of transparent acrylic plates, are inserted on two sides of the GDPs. Additionally, a stainless steel based sturdy end plate, featuring a cut-out window, can be engaged on two sides to compress the transparent PEM-FC and to prevent any bending of the titanium GDPs. The PEM-FC is secured in place using 4 screw joints, which are tightened to a consistent torque to ensure stability.

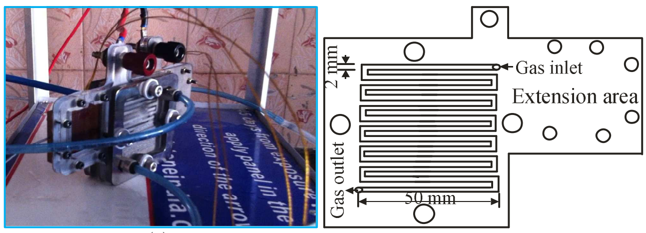

(a) (b)

Fig. 1: Block of (a) single transparent PEM-FC, (b) schematic of titanium GDP.

The transparent PEM-FC was subjected to rigorous testing at a specialized fuel cell test station, which was meticulously designed and constructed by Ingsman Energy & the FC Research Organization Pvt. Ltd in India, as depicted in Figure 2. This testing setup comprised oxygen and hydrogen cylinders, each fitted with pressure controllers, as well as controllers of mass flow for both gases. Humidifiers equipped with controllers of temperature were included to manage the reactants, alongside an electronic load and the transparent PEM-FC, which also had its own temperature control system. For the experimental procedures, high-purity hydrogen was procured from a metal hydride cylinder, while oxygen was sourced from a distinct cylinder. The flow rates for both hydrogen and oxygen were precisely controlled using AALBORG mass flow controllers, which facilitated flow rates ranging from 0 to 600.0ml/min for H_2 and 0 to 1000.0ml/min for O_2. An electronic load, rated at 10 volts and capable of handling 300amps, was connected to the transparent PEM-FC. Furthermore, for maintaining the humidification temperature of the reactants, temperature controllers are utilized and to regulate the temperature of the PEM-FC itself. Other parameters of the system are considered from [26-38].

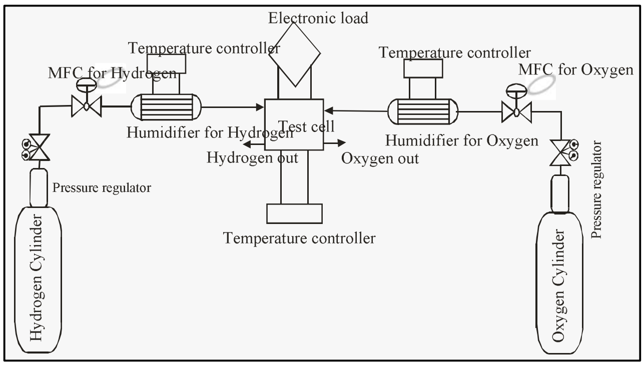

Fig. 2: Layout of experimental setup.

III. Results and Analysis

The optimal clamping pressure generated by the torque exerted on every bolt varied among various materials of GDL. This variation is attributed to their unique electro-physical characteristics, which include factors such as gas permeability, porosity, and the resistance between the collector to GDL. These characteristics are, in turn, affected by the clamping pressure applied. Hence, the main theme of this research is to determine the optimal torque or clamping pressure for every bolt to maximize the performance of PEM-FC. Furthermore, the study also investigated how different operating parameters including the operating and humidification temperatures of the PEM-FC, and the O_2 flow rate, impact the efficiency of the PEM-FC when the optimal torque is applied.

Case-1: Effect due to torque at bolt:

A series of studies were carried out through experiment to assess how varying torque affect the performance of the PME-FC. This was achieved by assign torque values that ranged from 2.0 to 3.5N.m, with increments of 0.5N.m for every bolt used in the assembly. During the experiments, the cathode humidification temperature (CHT) and the anode humidification temperature (AHT) are consistently maintained at 50° of temperature, while the fuel cell temperature (TFC) is set to 40°. The flow rate of the reactants is adjusted according to the measured current, which could be categorized as either low or high stoichiometry. High value refers to flow rates that are 2 times the amount needed for the measured current; specifically, this means providing 100% excess hydrogen for the hydrogen flow and 3.5 times the necessary amount for air flow. As a result, flow rates of the mass were managed to 100ml/min for H_2 and 200ml/min for O_2.

Data shown in Figure 3, represented as polarization curve, demonstrates that the performance enhances as the torque increases from 2.0 to 3.0N.m. This enhancement is primarily due to the fact that a higher bolt torque minimizes the resistance due to electrical contact between the GDL and the adjacent GDP, which in turn reduces the ohmic overpotential. Additionally, an increase in compression force affects the retention of water at the electrode plates and the area available for the electrochemical reaction, further contributing to a decrease in concentration overpotential. As a result demonstrated in Figure 3, the limiting density of current can rises from 0.18A/cm^2 at a torque of 2.0Nm to 0.3A/cm^2 at 3.0N.m. However, when the torque exceeds 3.0N.m, it causes a reduction in the thickness of the GDL, which subsequently decreases its permeability and porosity. This leads to a lower concentration of reactants at the reaction sites, which may account for the observed decline in PEM-FC performance beyond 3.0N.m, minimizing the dencity of current to 0.22A/cm^2 at 3.5N.m. In a similar manner, the peak power density rises from 0.0326W/cm^2 at a torque of 2.0Nm to 0.0685W/cm^2 at 3.0Nm, also moving to the right in conjunction with the increased density of current. This represents an improvement in the removal water rate at the membrane interface of cathode, effectively delaying the water flooding at the catalyst sites. The humidification temperatures for the anode and cathode were consistently maintained at 85°C and 75°C, respectively, while the PEM-FC temperature was controlled at 80°C.

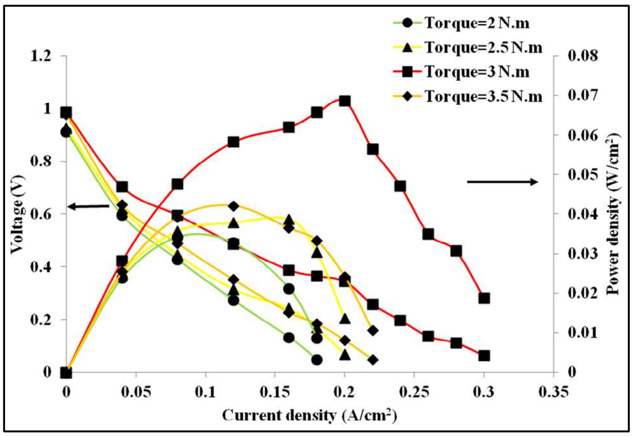

Fig. 3: Torque effect on bolts on the performance of the PEM-FC.

Case-2: Effect of AHT:

To explore how AHT affects the performance of PEM-FC at an optimal torque of 3.0N.m, two experimental studies were conducted at TFCs of 40°C and 80°C, with AHT changing from 40 to 80°C, as illustrated in Figure 4(a) and Figure 4(b) respectively. In both studies of experiments, the CHT is kept constant at 50°C, while the flow rates of mass for hydrogen and oxygen were adjusted at 100ml/min and 200ml/min. The curves revealed that an increase in AHT resulted in a decline in fuel cell performance; however, this decline was less significant at low and medium current flows, indicating that ohmic losses and activation remain relatively stable with rising AHT. In contrast, at higher current flows, the impact became more pronounced, showing a reduction in limiting current density as AHT increased. This effect is attributed to the fact that higher AHT results in increased content of net water on the anode side, which subsequently diminishes the back diffusion of water to the anode from the cathode.

Furthermore, the flow of water via the electro-osmotic drag mechanism also rises with an increase in AHT, leading to a greater accumulation of water on the cathode side. Hence, combined effect results in heightened flooding, which diminishes the limiting density of current and consequently impairs the fuel cell's response. Conversely, at lower AHT, the limiting current density rises due to an increase in hydrogen concentration on the anode side, which in turn decreases the anode water concentration. As a result, the concentration gradient of water between the anode and cathode increases, this not only alleviates flooding at the cathode but also enhances the performances of the cell. However, at AHT levels exceeding 60°C, the polarization curves nearly overlap, indicating that the PEM-FC performance doesn’t change significantly.

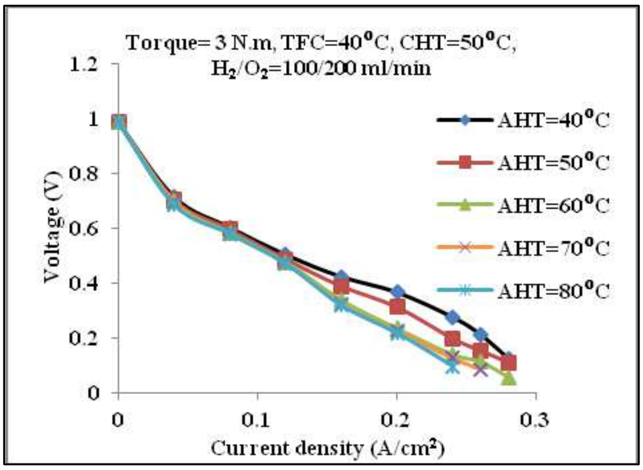

(a)

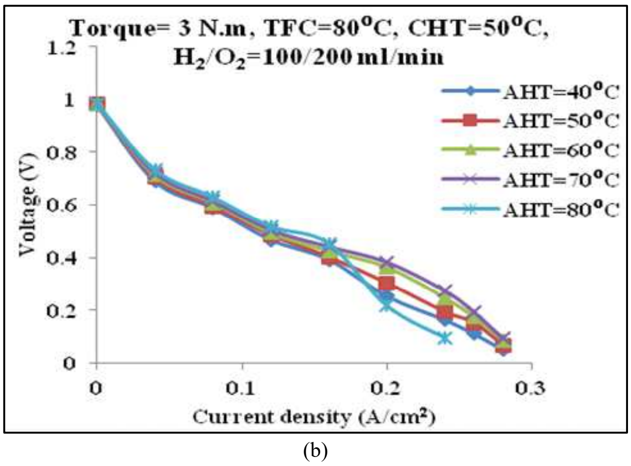

(b)

Fig. 4. AHT polarization curves at TFC= (a) 40°C; (b) 80°C.

When the PEM-FC will be operated at higher temperatures, specifically at 80°C, its performance showed improvement as the Anode AHT increased from 40°C to 70°C. However, a decline in performance was observed at 80°C, as depicted in Figure 4(b). The increase in the TFC led to a higher evaporation rate, which resulted in membrane dehydration on the anode side when the AHT was lower. As the current densities increased, the performance of the PEM-FC further enhanced due to the rise in the temperature with the water diffusion coefficient, which aided in the flow of water through back diffusion and helped prevent flooding at the cathode. As illustrated in Figure 4(b), at an AHT of 80°C, the fuel cell's performance experienced a significant drop, falling below 0.5 V. This reduction in performance can be linked to an increase in net electro-osmotic drag, which leads to an accumulation of excess water at the cathode side, ultimately decreases the overall efficiency of PEM-FC.

Case-3: Effect of CHT:

To explore how the CHT affects performance of a cell when the optimal torque of 3.0Nm, we varied the CHT to 80°C from 40°C. During this process, we kept the TFC constant at 40°C and the AHT at 50°C. Additionally, the mass flow rates for H_2 and O_2 were set at 100ml/min and 200ml/min, accordingly. The polarization curves illustrated in Figure 5 reveal a noticeable decrease in PEM-FC performance as the CHT rises from 40°C to 80°C. This performance drop is attributed to an increased volume of water being transported via the inlet oxygen to the interface of cathode. As a result, the gas stream's capacity to eliminate water through evaporation is compromised, which can lead to flooding at the interface of the cathode, even when the flow of current is low.

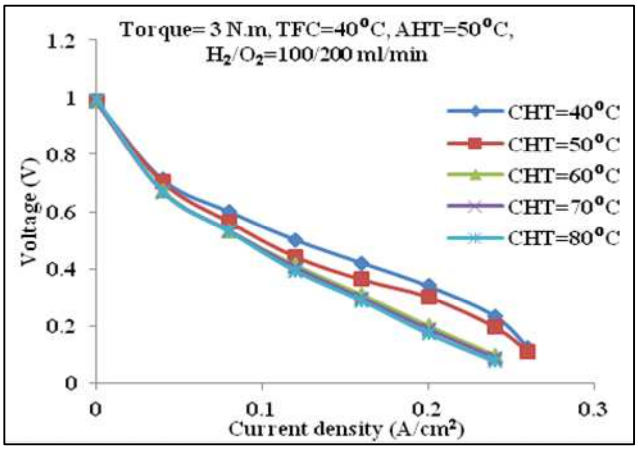

Fig. 5: Polarization curves at various CHTs.

Case-4: Effect of TFC:

To explore the effects of the TFC on its performance, we set the optimal bolt torque at 3.0N.m and varied the TFC from 40 to 80°C.

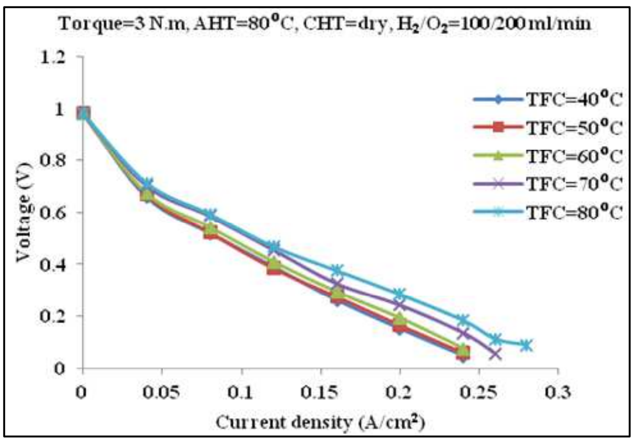

Fig. 6: Polarization curves at various TFCs.

During this investigation, the mass flow rates of hydrogen and oxygen were kept constant at 100ml/min and 200ml/min. The temperatures of the cathode and anode reactants will be maintained at 80°C and dry conditions, accordingly, to prevent the risk of anode side membrane dehydration at higher temperatures. As shown in the curves (Figure 6), both the limiting current density and performance of the PEM-FC improve with increasing TFC. Notably, the density of exchange current associated with the reaction of oxygen reduction experiences a significant increase as TFC rises, which in turn reduces activation losses. Higher temperatures within the cell enhance the proton conductivity of the membrane, leading to a decrease in losses due to ohmic resistance and facilitating better back diffusion of water. Furthermore, elevated cell temperatures boost the evaporation rate, which results in lower content of water on the cathode side, thereby alleviating concentration losses. The combined reduction in these three types of losses ultimately enhances the overall performance of the cell.

Case-5: Cathode flow rate reactant effect:

To explore how the flow rate of the reactant affects PEM-FC response at an optimal torque of 3.0N.m, we assessed 3 different flow rates of O_2: 300, 250, and 200 ml/min. The AHT was consistently maintained at 40°C, while the CHT was kept dry. The TFC was also set at 40°C, and flow rate of the hydrogen mass is fixed at 100ml/min. The polarization curves shown in Figure 7 clearly demonstrate that variations in oxygen flow rates have a minimal effect on both the activation and ohmic overpotential regions. This indicates that changes in oxygen supply do not significantly influence the performance characteristics in these specific areas. However, a significant impact was noted in the overpotential region concentration. It can be explained by the fact that an increase in the oxygen flow rate aids in the more efficient removal of cathode water, which in turn promotes the back diffusion of water to the anode from the cathode. This process ultimately enhances cell performance, particularly in the higher density of current region. The increased removal for rate of water correlates with the rise in cathode reactant flow rate, resulting in improved cell performance.

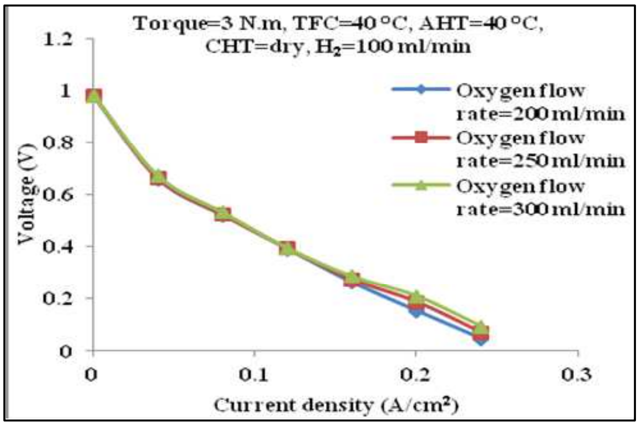

Fig. 7: Polarization curves during various flow rates of O_2.

IV. Conclusions

This research involved conducting experiments on a single transparent PEM-FC, which utilized titanium GDPs designed with a serpentine flow pattern. The primary objective was to investigate how optimized clamping pressure, determined by the torque applied to each bolt, along with various operating elements such as TFC, CHT, AHT, and the flow rates of the cathode reactants, influenced the performance of the PEM-FC. Due to increasing torque on each bolt, the resistance due to electrical contact between the GDL and the GDP decreased, leading to improved cell performance. However, if the torque continued to increase beyond a certain point, the permeability and porosity of the GDL were adversely affected, resulting in a decline in response of PME-FC. This interplay suggests that the fuel cell's performance initially improves up to a peak before it starts to reduce with further increases in torque at bolt. Additionally, when operating at a lower temperature of 40°C, the performance of the PEM-FC was found to decrease with rising AHT, whereas at a higher temperature of 80°C, performance improved with increasing AHT. This indicates the necessity of humidifying the anode stream to optimize PEM-FC performance. Furthermore, while the performance of the PEM-FC can be decreased by raising CHT, this effect became less pronounced at temperatures exceeding 60°C. In contrast, the performance of the PEM-FC showed improvement with higher TFC. As the temperature increased from 40 to 80°C, the limiting current density of the PEM-FC experienced a significant rise, increasing from 240mA/cm^2 to 280mA/cm^2.

References

[1]. Jianwei Li, "A New Fuel Cell Degradation Model Indexed by Proton Exchange Membrane Thickness Derived From Polarization Curve", IEEE Transactions on Transportation Electrification (Volume: 9, Issue: 4, December 2023), https://doi.org/10.1109/TTE.2022.3188727.

[2]. P. Salodkar, S. Meshram and S. Dey, "Static PEMFC Model Simulation to Exhibit the Working with Converter," 2022 2nd International Conference on Emerging Frontiers in Electrical and Electronic Technologies (ICEFEET), Patna, India, 2022, pp. 1-5, doi: 10.1109/ICEFEET51821.2022.9848132.

[3]. J. Li, D. Zhao, L. Xie, Z. Zhou, L. Zhang and Q. Chen, "Internal water content estimation for PEM fuel cell utilizing adaptive sliding mode technology," in CSEE Journal of Power and Energy Systems, doi: 10.17775/CSEEJPES.2024.00770.

[4]. T. Akiki, G. Accary, W. Charon and R. Kouta, "Influence of local porosity, local permeability, and contact resistance between the gas diffusion layer and the bipolar plate, on the performances of a polymer electrolyte membrane fuel cell," CCCA12, Marseille, France, 2012, pp. 1-6, doi: 10.1109/CCCA.2012.6417893.

[5]. M. Kandidayeni, H. Chaoui, L. Boulon and J. P. F. Trovão, "Adaptive Parameter Identification of a Fuel Cell System for Health-Conscious Energy Management Applications," in IEEE Transactions on Intelligent Transportation Systems, vol. 23, no. 7, pp. 7963-7973, July 2022, doi: 10.1109/TITS.2021.3074903.

[6]. R. Kumar and K. A. Subramanian, "Study of Surface Morphology of Electrodes (Gas Diffusion Layer) and Bipolar plates in PEM fuel cell," 2022 IEEE North Karnataka Subsection Flagship International Conference (NKCon), Vijaypur, India, 2022, pp. 1-4, doi: 10.1109/NKCon56289.2022.10127046.

[7]. Ge J, Higier A, Liu H. Effect of gas diffusion layer compression on PEM fuel cell performance. Journal of Power Sources 2006; 159:922-27.

[8]. Yang, Q.; Wang, X.; Xiao, G. Clamping Pressure and Catalyst Distribution Analyses on PEMFC Performance Improvement. *Energies* **2024**, *17*, 5223, doi:10.3390/en17205223.

[9]. Busra Yilgin, Cenk Celik, Fatma Gul Boyaci San, "Clamping effects on the performance of proton exchange membrane fuel cell", International Journal of Hydrogen Energy, Volume 141, Pages 888-895, 2025, https://doi.org/10.1016/j.ijhydene.2024.12.015.

[10]. Kaoutar Kabouchi; Mohamed Karim Ettouhami, "Simulation of PEM Fuel Cell Stack Performance Under Varying Voltage Conditions Using CFD", 2025 5th International Conference on Innovative Research in Applied Science, Engineering and Technology (IRASET),

26 May 2025, Fez, Morocco, https://doi.org/10.1109/IRASET64571.2025.11008028.

[11]. Arife Uzundurukan, Muhittin Bilgili, Yılser Devrim, "Examination of compression effects on PEMFC performance by numerical and experimental analyses", International Journal of Hydrogen Energy, Volume 45, Issue 60, Pages 35085-35096, 2020, https://doi.org/10.1016/j.ijhydene.2020.04.275.

[12]. DongWoong Choi, "Electrochemical behavior and compression force analysis for proton exchange membrane fuel cells with different reaction areas", International journal of Energy Research, September 2021, https://doi.org/10.1002/er.7236.

[13]. A. Molavi, M. Serra Prat and A. P. Husar, "Improved Supervisory Controller Design for a Fuel Cell Hybrid Electric Vehicle," in IEEE Transactions on Vehicular Technology, vol. 73, no. 4, pp. 4918-4933, April 2024, doi: 10.1109/TVT.2023.3331242.

[14]. Z. Sun, Y. Nie, Y. Wang and Z. Chen, "Multiphysics Field Virtual Sensors for PEM Fuel Cells Based on a Deep Learning Method," in IEEE Transactions on Instrumentation and Measurement, vol. 74, pp. 1-11, 2025, Art no. 1009611, doi: 10.1109/TIM.2025.3565057.

[15]. M. Dhimish and V. Lazarov, "Assessing Durability in Automotive Fuel Cells: Understanding the Degradation Patterns of PEM Fuel Cells Under Variable Loads, Temperature, Humidity, and Defective Stack Conditions," in IEEE Transactions on Transportation Electrification, vol. 11, no. 1, pp. 3091-3101, Feb. 2025, doi: 10.1109/TTE.2024.3434609.

[16]. R. Song, Z. Wei, F. Pan and C. Zhang, "Anodic Cold Start Control of PEM Fuel Cell System With Temperature-Dependent Solenoid Valve Model," in IEEE Transactions on Transportation Electrification, vol. 11, no. 3, pp. 7300-7308, June 2025, doi: 10.1109/TTE.2025.3526184.

[17]. C. Harish et al., "Novel Energy Management System for Microgrid Supplied by Various Renewable Energy Sources," 2025 International Conference on Computing Technologies (ICOCT), Bengaluru, India, 2025, pp. 1-6, doi: 10.1109/ICOCT64433.2025.11118719.

[18]. K. Mondal et al., "Super Twisting Sliding Mode Controllers based Grid Connected Hybrid Renewable Energy Sources Operated Power Supply System," 2025 International Conference on Computing Technologies (ICOCT), Bengaluru, India, 2025, pp. 1-7, doi: 10.1109/ICOCT64433.2025.11118849.

[19]. K. Krishnaveni et al., "Enhancement of Power Quality for PV-Wind-SMES-FC-AE-Battery based Standalone Microgrid," 2025 International Conference on Computing Technologies (ICOCT), Bengaluru, India, 2025, pp. 1-6, doi: 10.1109/ICOCT64433.2025.11118909.

[20]. S. C. Kalshetti et al., "Coordinated Energy Management of Smart Grid Powered by Hybrid Renewable Power Sources at Various Locations", *2024 International Conference on Sustainable Power & Energy (ICSPE)*, Raigarh, India, 2024, pp. 1-6, doi: 10.1109/ICSPE62629.2024.10924364.

[21]. Kandi Bhanu Prakash, Suresh Kakinatla, Sankara Rao Burada and Siva Ganesh Malla, "Hybrid Renewable Energy Sources based Mobile Charging Unit for Public Usage", *E3S Web of Conferences*, Vol. 540, No. 01001, June 2024, DOI: https://doi.org/10.1051/e3sconf/202454001001.

[22]. Malla, Priyanka, Malla, Siva Ganesh and Calay, Rajnish Kaur, "Voltage control of standalone photovoltaic – electrolyzer- fuel cell-battery energy system", *International Journal of Emerging Electric Power Systems*, Vol. 24, No. 5, 2023, pp. 649-658. https://doi.org/10.1515/ijeeps-2022-0047.

[23]. Balu, Vankudothu and Krishnaveni, K and Malla, Priyanka and Malla, Siva Ganesh, "Improving the power quality and hydrogen production from renewable energy sources based microgrid", *IOP: Engineering Research Express*, Vol. 5, No. 3, Aug. 2023, DOI: https://dx.doi.org/10.1088/2631-8695/acecdb.

[24]. S. G. Malla, K. Al Jaafari, K. A. Hosani and U. R. Muduli, "Improvement of Power Quality through SMES Control in a Standalone Hybrid Microgrid System", *2023 IEEE IAS Global Conference on Emerging Technologies (GlobConET)*, London, United Kingdom, 2023, pp. 1-6, doi: 10.1109/GlobConET56651.2023.10150007.

[25]. S. S. Prasad, et al., "Novel Control Scheme for Wind based Standalone Hybrid Power Generation System under Faults on Three Phase Distribution Feeders", *2023 7th International Conference on Computing Methodologies and Communication (ICCMC)*, Erode, India, 2023, pp. 21-26, doi: 10.1109/ICCMC56507.2023.10084134.

[26]. Y. I. P. Darshini, et al., "Power Quality Improvement of Standalone Microgrid during Faults on Distribution Line with DSTATCOM", *2023 5th International Conference on Smart Systems and Inventive Technology (ICSSIT)*, Tirunelveli, India, 2023, pp. 530-536, doi: 10.1109/ICSSIT55814.2023.10061071.

[27]. T. Anuradha et al., "Power Quality Improvement of Hybrid Standalone Microgrid with DSTATCOM during Faults on Distribution Line", *2022 IEEE International Conference on Power Electronics, Drives and Energy Systems (PEDES)*, Jaipur, India, 2022, pp. 1-7, doi: 10.1109/PEDES56012.2022.10080027.

[28]. Malla, Siva Ganesh, et al., "Coordinated power management and control of renewable energy sources based smart grid", *International Journal of Emerging Electric Power Systems*, Vol. 23, No. 2, 2022, pp. 261-276. https://doi.org/10.1515/ijeeps-2021-0113.

[29]. C. Pradhan, M. K. Senapati, S. G. Malla, P. K. Nayak and T. Gjengedal, "Coordinated Power Management and Control of Standalone PV-Hybrid System With Modified IWO-Based MPPT", *IEEE Systems Journal*, Vol. 15, No. 3, pp. 3585-3596, Sept. 2021, doi: 10.1109/JSYST.2020.3020275.

[30]. M. R. Prasada Reddy et al., "3DOF-PID Controllers for Regulation of Voltage in Microgrid Pored by Hybrid Wind - PV - Battery - AE-FC," 2025 International Conference on Computing Technologies (ICOCT), Bengaluru, India, 2025, pp. 1-7, doi: 10.1109/ICOCT64433.2025.11118930.

[31]. G. S. Babu et al., "Novel Control Method for Wind-Hydrogen-Battery based Standalone Microgrid under Faults on Distribution Lines," 2025 International Conference on Computing Technologies (ICOCT), Bengaluru, India, 2025, pp. 1-6, doi: 10.1109/ICOCT64433.2025.11118914.

[32]. T. Jena et al., "Improvement of Power Quality by using TSK-Fuzzy Controllers in Wind and Photovoltaic based Hybrid Nanogrid," 2025 International Conference on Computing Technologies (ICOCT), Bengaluru, India, 2025, pp. 1-6, doi: 10.1109/ICOCT64433.2025.11118792.

[33]. F. Albtoush et al., "Enhancement of Power Quality in a Standalone PV-Wind-Battery Hybrid Microgrid with ANN-LSTM Controllers", *2025 First International Conference on Advances in Computer Science, Electrical, Electronics, and Communication Technologies (CE2CT)*, Bhimtal, Nainital, India, 2025, pp. 718-723, doi: 10.1109/CE2CT64011.2025.10939083.

[34]. S. G. Malla, J. Dadi and P. K. Dadi, "Solar-hydrogen energy based hybrid electric vehicle," 2017 International Conference on Energy, Communication, Data Analytics and Soft Computing (ICECDS), Chennai, India, 2017, pp. 129-137, doi: 10.1109/ICECDS.2017.8389673.

[35]. S. G. Malla and R. K. Vadrevu, "Novel controller scheme for grid connected fuel cell," 2016 International Conference on Electrical, Electronics, and Optimization Techniques (ICEEOT), Chennai, India, 2016, pp. 4425-4430, doi: 10.1109/ICEEOT.2016.7755555.

[36]. M. Taufiqurrohman and D. Octaviani, "Portable Pico Hydro Power Plant for Power Station Charger", *Vokasi Unesa Bull. Eng. Technol. Appl. Sci.*, vol. 1, no. 2, pp. 1–11, Dec. 2024.

[37]. A. M. Obais and A. A. Mukheef, "Design of a 120V, 5A SEPIC DC-DC Converter for Unipolar 120V DC Microgrid ", *Vokasi Unesa Bull. Eng. Technol. Appl. Sci.*, vol. 2, no. 3, pp. 655–665, Sep. 2025.

[38]. Anantwar, H., & Sunda, S. (2023). Intelligent Optimized Voltage Control for Hybrid Off-Grid Power Systems. *Journal of Asian Energy Studies*, *7*, 39–47. https://doi.org/10.24112/jaes.070003